Strain Tuning of Excitons in Monolayer WSe_2

Ozgur Burak Aslan, Minda Deng, Tony F. Heinz

Department of Applied Physics, Stanford University, Stanford, California 94305, USA and

SLAC National Accelerator Laboratory, Menlo Park, California 94025, USA

Manuscript

1. Text

\begin{abstract}

\begingroup

\obeylines

We investigate excitonic absorption and emission in monolayer (1L) WSe_2 under tensile strain. We observe a redshift of 100 meV in the A exciton energy and a decrease of 25 meV in its estimated binding energy under 2.1% strain. Surprisingly, the linewidth of the A exciton decreases by almost a factor of two under strain, from 42 to 24 meV at room temperature. We explain this effect as the result of suppression of phonon-mediated exciton scattering channels. We show that such a suppression results from the relative shift under strain of a secondary valley in the conduction band that is nearly degenerate with the K valley where the A exciton is formed.

\endgroup

\end{abstract}

\pacs{63.20.-e, 71.35.-y, 73.22.-f, 78.67.-n}

\maketitle

\section{Introduction}

Excitons dominate the optical spectra of atomically thin semiconducting transition metal dichalcogenides (TMDCs) due to their high binding energy and oscillator strength [1,2]. It is, thus, invaluable to understand them for many-body physics and fundamental studies on TMDCs. The ability to tune them is, moreover, very valuable for optoelectronic applications. Recent studies have demonstrated the tunability of the optical gaps and excitonic binding energies by 10s of meV via external control such as electrical gating, magnetic fields, and dielectric screening [3-7]. Strain tuning, another external control, has been repeatedly employed to engineer the optical spectra of monolayer (1L) TMDCs [8-15]. Redshifts of more than 400 meV in the optical gap [8], indirect to direct gap transitions [10], and changes in the spectral linewidths via strain have been reported in TMDCs [11,12,15-17]. In contrast, the influence of strain tuning of their electrical (quasiparticle) band gaps or of excitonic binding energies has not yet been investigated. Moreover, the effect of strain on other optical fingerprints such as linewidth has not yet been modeled or fully understood.

\begin{figure*-RCB-

\includegraphics{Figure_1-RCB-

\caption{\protect\input{caption_1.txt}}

\label{fig:Fig1-RCB-

\end{figure*}

\section{Strain as a Probe}

Strain can provide a means of probing the band structure of monolayers and the relative disposition of different minima in the conduction band (CB). 1L TMDCs are expected to possess direct gaps, but with indirect gaps only a few 10s to 100s of meV higher in energy [18-20]. Therefore, the optical and electrical properties of 1Ls may be strongly influenced by the exciton- and carrier-phonon scattering between valleys at room and elevated temperatures [19,21-23]. It has been proposed that tensile strain can alter the energy separation between those two states associated with the direct and indirect gaps, affecting the scattering rates [24-27]. Consequently, we expect that the altered energy separation under strain may lead to observable fingerprints in the optical spectra of the material. In this manner, strain can provide a means of optically probing the indirect gap, which is difficult to probe by optical spectroscopy when its energy is very close to that of the direct gap.

\section{Methods}

In this study, we apply uniaxial tensile strain to 1L WSe_2 and perform in-situ optical absorption and photoluminescence (PL) spectroscopy (see the Supplemental Material (SM) sections S1 and S2 [28]). We extract the peak positions of the excitonic states and infer the changes in the excitonic binding energy induced by strain. We note a significant decrease in the spectral linewidths of the excitons. Despite the similar dependence of the material properties on strain, we observe quantitatively different line narrowing in 1L WS_2. We consider the strain dependence of the linewidth of the lowest lying exciton (KK or A exciton) and show that the different narrowing can be explained by reduced phonon-mediated intervalley scattering rate from the direct to the lowest lying indirect (KQ (also known as $K\Lambda$)) excitonic state. By making use of the strain dependence of the excitonic gaps and binding energies observed, we calculate the strain-dependent intervalley scattering rate within the deformation potential approximation. We then give an estimate for the separation between the KK and KQ excitons, which has been examined in recent studies [29-31]. It is important to note that we refer to the spin-allowed states with respect to the top of the K point in valence band (VB) for the A exciton in this paper, which are higher and lower energy spin-states of the K and Q valleys in CB, respectively [18].

\section{Choice of Materials}

We focus our attention on WSe_2 and WS_2 due to their large VB spin-orbit coupling. This enables the ready observation of the ground state and the excited states of the A exciton without the complication of the presence of the relatively broad B exciton in the critical spectral range. Moreover, the relatively small separation between the KK and KQ states makes the optical spectra of the excitons more sensitive to strain than systems such as MoS_2 and $MoSe_2$ which have been widely studied in strain-optics experiments [8,9,12-14,18].

\section{Strain-tuned Absorption and PL Spectra}

We plot the effect of strain on the absorption and PL of 1L WSe_2 in Figure 1. The absorption spectra show that the A exciton redshifts from 1.67 eV to 1.57 eV and B exciton redshifts from 2.08 eV to 2.00 eV as the strain increases from 0.0% to 2.1%. The strain-induced redshifts are far greater than the exciton linewidths, allowing the ready identification of the influence of strain. Strain-dependent PL spectra confirm the redshift of the A exciton, verifying that the emission and absorption originate from the same physical transition. The amplitudes of the absorption and PL peaks of the A exciton increase by about 75%. Surprisingly, all the features observed become narrower. Specifically, the linewidths of the A exciton absorption and emission peaks decrease from 42 to 24 meV for 2.1% strain. In addition to the strong 1s state of the exciton (A_{1s}), we are also able to observe the 2s (A_{2s}) and 3s (A_{3s}) excited states, which become more pronounced under strain. Despite the spectral narrowing, oscillator strengths of the A exciton absorption and PL peaks

(integrated areas under the peaks) are found to be nearly insensitive to strain as shown in Figure 1c and Figure 1d, respectively. (see SM section S3 for more absorption spectra [28])

\section{Analysis}

We analyze the strain-dependent absorption spectra and extract the peak positions of the excitons by fitting to Lorentzian lineshapes [1]. We plot the energy separations between the A_{2s} and A_{1s} (E_{2s-1s}), and B and A excitons (E_{B-A}) and their linear fits in Figure 1(e) and Figure 1(f), respectively. We obtain from the fit that E_{2s-1s} decreases from 157(±1) meV by 6(±1) meV/% strain. We estimate the change in the exciton binding energy as twice E_{2s-1s} and find that it decreases from 315(±2) meV by 12(±2) meV/% strain [1,4]. This corresponds to a decrease of 3.8(±0.6)% per % strain. This is in good agreement with the calculations of the strain dependence of the exciton binding energy as arising from a decrease in the exciton reduced mass [32,33]. We note that these analyses assume that the binding energy scales linearly with the reduced mass. However, for a binding energy scaling as the reduced mass, for instance, to the power 0.3 [34], the experimental data would imply a rate of decrease of the reduced mass with strain (>10% per % strain) exceeding the predicted rate. A and B excitons redshift at different rates so that E_{B-A} increases from 409 meV by 10 meV/% strain mainly due to the increase in the splitting of the top of VB at the K point [35,36], (see SM section S7 [28]).

\begin{figure*}-RCB-

\includegraphics{Figure_2-RCB-

\caption{\protect\input{caption_2.txt}}

\label{fig:Fig2-RCB-

\end{figure*}

We next consider the strain-dependent linewidths of the A and B excitons. In Figure 2a, we plot the linewidths for the absorption features in WSe_2 as well as WS_2. The linewidth of the A (B) exciton of WSe_2 decreases from 42 (170) meV at 0.0% strain to 24 (146) meV at 2.1% strain. We observe a quantitatively different narrowing for WS_2: The linewidth of its A (B) exciton decreases from 30 (127) meV at 0.0% strain to 24 (119) meV at 1.5% strain and remains nearly invariant around 24-25 meV up to 2.3% strain.

\section{Discussion}

\subsection{Effect of Strain on Linewidths}

Here, to discuss the surprising strain-driven decrease in the A exciton linewidth, we note that it is determined principally by three processes [22]: Radiative decay (γ_{rad}), intravalley scattering (KK to KK exciton-phonon scattering; γ_{KK-KK}) and intervalley scattering (KK to KQ exciton-phonon scattering; γ_{KK-KQ}) rates. We may disregard the KK to KK' and KK to ΓK intervalley scattering processes, since their rates are understood to be relatively low, mainly due to the relatively small deformation potentials of the associated scattering mechanisms [19,22]. Let us now consider the effect of strain on these contributions. First, γ_{rad} of 1L WSe_2 and MoS_2 has been calculated to increase by about 10% per % strain [32]. We assume the same trend for WSe_2. The effect of strain on γ_{rad} is plotted as the yellow area in Figure 2(b) and Figure 2(c). The predicted change in linewidth from γ_{rad} is slight and opposite to the overall trend [22,32,37]. Secondly, to analyze γ_{KK-KK}, we employ the recently reported effective deformation potential model of 1L TMDCs [19]. We consider the strain-induced change in the KK exciton reduced mass, mass density of the material, sound velocity and the related phonon frequencies [20,32,38]. We find that γ_{KK-KK} decreases by about 2 (2)% per % strain for WSe_2 (WS_2), corresponding to a decrease of less than 1 meV at the highest strain achieved, plotted as the orange area in

Figure 2(b) (Figure 2(c)) [22]. The effect of strain on γ_{KK-KK}, as well as on γ_{rad}, is clearly not sufficient to account for the significant reduction observed in the linewidths (orange lines in Figure 2(b) and Figure 2(c)).

We thus infer that influence of strain on γ_{KK-KQ} must account for the majority of the decrease in linewidth in both WSe_2 and WS_2. We propose that origin of the strong strain dependence of γ_{KK-KQ} arises from the near degeneracy of the KK and KQ excitons, so that slight shifts in the relative positions of the valleys can have a dramatic impact on scattering rates. In fact, the energy separation between the KQ and KK states, E_{KQ-KK}, is expected to increase due to weaker (stronger) coupling between the orbitals contributing to the K (Q) point of CB under tensile strain [24-27,39]. Such a shift in the relative energies of the states can lead to a rapid decrease in the scattering rate due to a reduction in the density of available final states in the scattering process [24]. We show this effect schematically in Figure 2(d).

Here we develop a model to analyze the strain dependence of γ_{KK-KQ}. We must first consider the strain-dependent E_{KQ-KK}. Writing the contributions to the exciton energy in terms of shifts of the band separation and shifts of the exciton binding energy, under strain ε

$$E_{KQ-KK}(\varepsilon) = E_{KQ}(\varepsilon) - E_{KK}(\varepsilon) = E_{KQ-KK}(0) + \Delta E_{KQ}^{quasiparticle}(\varepsilon) - \Delta E_{KQ}^{binding}(\varepsilon) - \Delta E_{KK}(\varepsilon) \quad (1)$$

Here $E_{KQ}(\varepsilon)$ and $E_{KK}(\varepsilon)$ are the strain-dependent energies of the KQ and KK excitons, respectively. $\Delta E_{KQ}^{quasiparticle}(\varepsilon)$, $\Delta E_{KQ}^{binding}(\varepsilon)$, and $\Delta E_{KK}(\varepsilon)$ are the changes induced by strain in the KQ quasiparticle gap, KQ exciton binding energy, and the KK exciton energy, respectively. We evaluate these quantities for WSe_2 in the following manner. $\Delta E_{KK}(\varepsilon)$ = -47 meV/% strain is obtained directly from the experimental absorption spectra presented above. $\Delta E_{KQ}^{binding}(\varepsilon)$ can be estimated from the change of the KQ exciton reduced mass with strain (see SM section S7 [28]); we find $\Delta E_{KQ}^{binding}(\varepsilon)$ = -6 meV/% strain [20,32,36]. We extract $\Delta E_{KQ}^{quasiparticle}(\varepsilon)$ = 15 meV/% strain from density functional theory (DFT) calculations in the literature [10]. Combining these results, we obtain for the strain dependence of the relative energies of indirect and direct excitons

$$E_{KQ-KK}(\varepsilon) = E_{KQ-KK}(0) + 68\ meV\frac{\varepsilon}{\%} \quad (2)$$

The lack of significant enhancement of the PL with strain (Figure 1(d)) indicates that $E_{KQ-KK}(0) \gtrsim k_B T$, where k_B and T are Boltzmann constant and room temperature, respectively. If this were not the case, an increased E_{KQ-KK} at higher strain would result in significantly more KK excitons in thermal equilibrium and thus stronger PL. This view is compatible with nearly direct-gap optical excitations in 1L WSe_2 and WS_2 at room temperature that become more direct under tensile strain (see SM section S1 [28] for a discussion of the PL intensity under strain). We note that at higher strain, γ_{KK-KQ} is expected to diminish and thus the total linewidth will be dominated by γ_{KK-KK} and γ_{rad}. Thus, we infer that they contribute in total about 20 meV to the linewidth [40] which we account for to deduce γ_{KK-KQ}. We estimate $E_{KQ-KK}(0) = 40$ (100) meV and, our model fits the strain dependent linewidth reasonably well with γ_{KK-KQ} decreasing from 21 (9) meV to 5 (4) meV for WSe_2 (WS_2), shown as the turquoise area in Figure 2b (c). A higher value for E_{KQ-KK} for WSe_2 than WS_2 is consistent with the DFT calculations, since the two materials have comparable exciton binding energies [18]. Therefore, we estimate the lowest lying indirect gaps, E_{KQ}, of unstrained 1L WSe_2 and WS_2 to be 1.71 eV and 2.10 eV, respectively (see SM section S5 [28]).

\subsection{WS\lowercase{e}$_{\mathrm {2}}$ vs WS$_2$ }

The material properties of WSe_2 and WS_2 show generally similar trends with strain. However, we have observed that the linewidth narrowing observed is significantly larger in WSe_2 (18 meV, 40% of the unstrained linewidth) than in WS_2 (6 meV, 20% of the unstrained linewidth), both of which are much larger than the magnitude of the applied strain. This observation further supports the essence of our model that a different value of $E_{KQ-KK}(0)$ (40 meV vs 100 meV) and an increase in E_{KQ-KK} can result in decreases of γ_{KK-KQ} that are relatively much greater than strain and are significantly different for WSe_2 and WS_2. Similar effects were reported in conventional semiconductors, such as Ge and GaAs, when excitonic binding energies and intervalley scattering were manipulated by external pressure [41,42].

\subsection{Linewidths of Other Excitons}

The linewidth of the B exciton, as well as of the excited states of the A exciton, are larger than the A_{1s} exciton linewidth. These states lie higher in energy enabling relaxation channels beyond those presented above. Nevertheless, we expect that the intervalley scattering rate γ_{KK-KQ} of the aforementioned excitons should also decrease with strain due to the relative shifts of the higher lying KK and KQ states. Experimentally, we do indeed observe a decrease of 24 (8) meV in the B exciton linewidth of WSe_2 (WS_2) at high strain. However, a detailed and quantitative model to explain the linewidth narrowing observed for those excitons with strain is beyond the scope of this paper [43].

\begin{figure-RCB-

\includegraphics{Figure_3-RCB-

\caption{\protect\input{caption_3.txt}}

\label{fig:Fig3-RCB-

\end{figure}

\section{Strained vs Unstrained WS\lowercase{e}$_{\mathrm {2}}$}

The overall effect of strain on 1L WSe_2 is presented in Figure 3a, in which the absorption spectra of the strained and unstrained 1L are illustrated schematically. Unstrained 1L WSe_2 at room temperature has a ground state A exciton at 1.67 eV with a binding energy of 315 meV and a linewidth of 42 meV and a quasiparticle gap of 1.98 eV (blue curve in Figure 3(a)). 2.1% strained 1L WSe_2 possesses a ground state A exciton at 1.57 eV with a linewidth of 24 meV and a quasiparticle gap of 1.86 eV (red curve in Figure 3). We note that the linewidth of the strained WSe_2, 24 meV, is significantly smaller than that of the recently reported hBN encapsulated samples, 32 to 34 meV [44]. The energy separation between the lowest energy direct and indirect gap states is about 145 meV larger than the unstrained case. As a result, the ground and excited states of the A exciton are narrower and more noticeable due to weaker exciton-phonon coupling. The strain dependence of the peak positions of the A exciton $1s$, $2s$, quasiparticle band gap and KQ exciton are shown in Figure 3b.

\section{Implications}

Spin and valley lifetime of excitons and electrons are expected to be longer in strained 1L WSe_2 and WS_2 since intervalley scattering is strongly suppressed. Due to the increased coherence lifetime of excitons and other tunable characteristics, strained 1Ls yield heterostructures with superior optoelectronic properties [45-49]. Moreover, higher mobility is expected from the devices made from strained 1L TMDCs due to decreased carrier-phonon intervalley scattering [20,24], as in the case of strained silicon [50].

\section{Summary}

In summary, we have manipulated the optical signatures of the excitons of 1L WSe_2 and WS_2 via mechanical strain. We have lowered the optical band gap of 1L WSe_2 by 100 meV, resulting in an absorption spectrum distinct from the unstrained 1L. We have deduced that the exciton binding energy decreases by 25 meV as a result of lower exciton

reduced masses, implying a decrease of 125 meV in its quasiparticle band gap. We have demonstrated that the pronounced observed narrowing in the exciton linewidth can be explained on the basis of an increased energy separation between the indirect (KQ) and direct (KK) gaps, suppressing the phonon-induced intervalley scattering. Our results suggest that, compared to WS_2, WSe_2 has a smaller indirect-direct gap separation. As a result, a larger portion of the excitonic linewidth in 1L WSe_2 is due to intervalley scattering as a result and the A exciton linewidths reach the same value of 24 meV at high strain. Further studies in a regime of still higher mechanical strain [40,51], should not only yield stronger tuning of energies, but also lead to further insight into the scattering and many-body physics of 2D excitons.

2. Figures

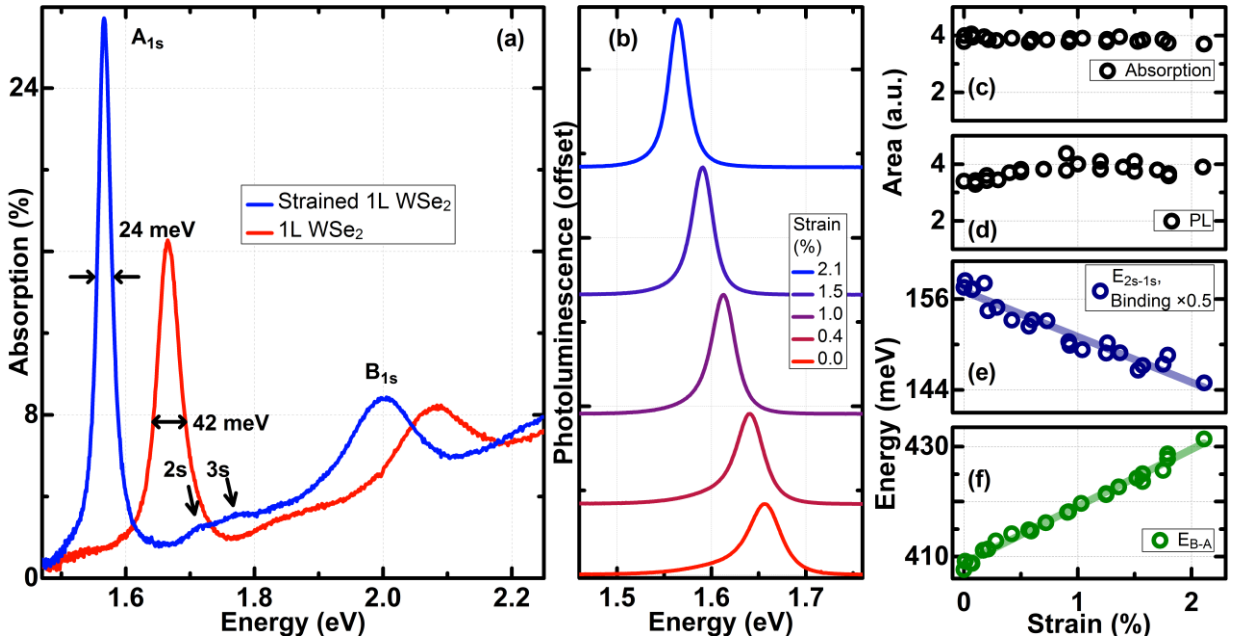


Figure 1: (a) Absorption spectra of 2.1% strained and unstrained 1L WSe_2. (b) Strain-dependent PL spectra of 1L WSe_2 (offset). Strain dependence of the strength of (c) absorption and (d) PL due to the A_{1s} exciton; (e) E_{2s-1s}, and A exciton binding energy; (f) E_{B-A}. Hollow circles are data points and solid lines are corresponding linear fits in (c)-(f).

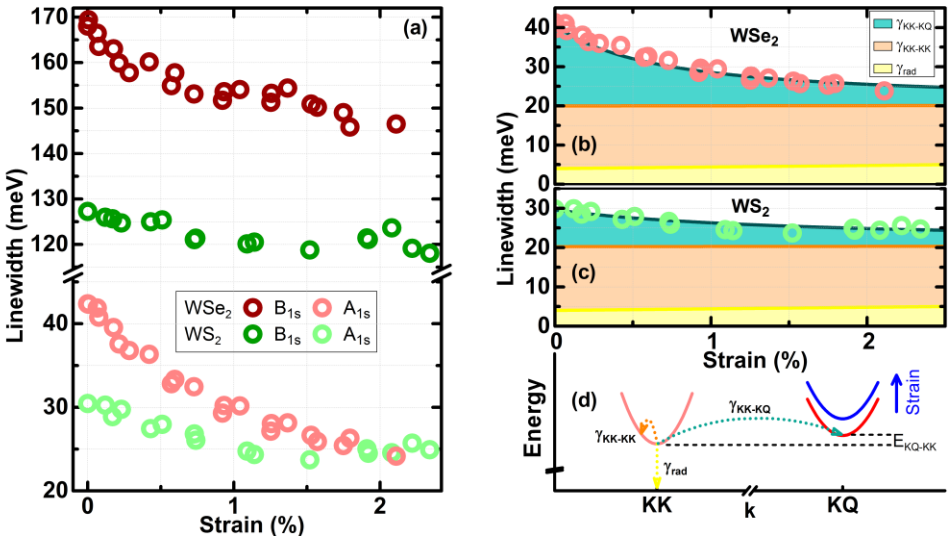


Figure 2: (a) Experimentally measured strain dependence of the total linewidths of the A and B excitons in 1L WSe_2 and WS_2. Strain dependence of the extracted homogeneous linewidths and calculated contributions to the A exciton linewidth in 1L (b) WSe_2 and (c) WS_2 (see SM section S8 [28]). The height of the colored areas between the solid lines represents the contributions from the radiative decay γ_{rad} (yellow), intravalley exciton-phonon scattering γ_{KK-KK} (orange), intervalley exciton-phonon scattering γ_{KK-KQ} (turquoise). (d) Schematic representation of the line broadening mechanisms and the strain dependence of the relative energy levels of KQ and KK states.

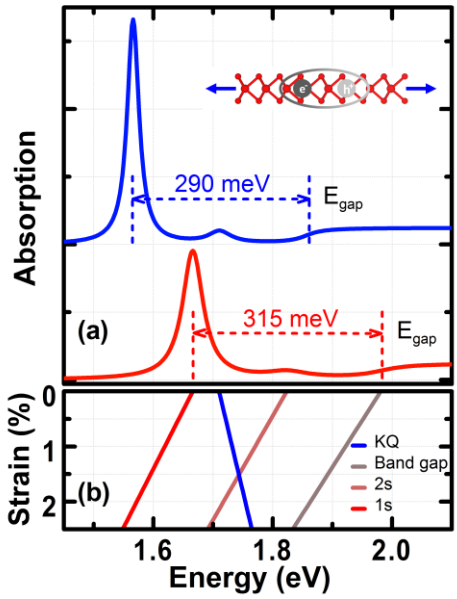


Figure 3: (a) Schematic illustration of the absorption spectra of strained (top, offset, in blue) and unstrained (bottom, in red) 1L WSe_2 due to the A exciton. Vertical dashed lines denote the position of the $1s$ state (left) and quasiparticle band gap (right). For clarity, only the $2s$ state among the excited excitonic states is shown. (b) Calculated strain-dependent positions of the A exciton $1s$, $2s$ states, quasiparticle band gap and KQ state.

Acknowledgements

The experimental studies were supported by the National Science Foundation's MRSEC program through Columbia in the Center for Precision Assembly of Superstratic and Superatomic Solids (DMR-1420634). Analysis was supported by the Department of Energy, Office of Science, Basic Energy Sciences, Materials Sciences and Engineering Division, under Contract DE-AC02-76SF00515.

Supplemental Material

Table of Contents

S1 Sample Fabrication and Optical Measurements 9

S2 Applying Strain to PETG and WSe_2, and Its Calculation 11

S3 Strain-dependent Absorption Spectra of 1L WSe_2 11

S4 Strain Dependence of the KK Quasiparticle Gap for 1L WSe_2 12

S5 Linewidth as a function of $KQ - KK$ separation for 1L WSe_2 and 1L WS_2 12

S6 $KQ - KK$ Separation for 1L and Few-layer WSe_2 13

S7 Strain Dependence of the Binding energy of the KQ and B excitons, and B-A splitting 13

S8 Strain Dependence of Stokes Shift and Estimating the Inhomogeneous Broadening 14

S9 Effect of hBN Encapsulation on the Exciton Linewidths 15

S10 Orientation Dependence of Applied Strain 15

S11 Built-in or Temperature-Driven Strain, Dielectric Screening 15

S1 Sample Fabrication and Optical Measurements

We mechanically exfoliate 1L WSe_2 and WS_2 from bulk crystals onto polydimethylsiloxane (PDMS) substrates [52]. Firstly, we perform absorption and PL measurements. Secondly, we transfer the 1Ls onto a 1.0 mm thick flexible polymer, polyethylene terephthalate glycol-modified (PETG). Next, by bending the PETG via a micromanipulator, we incrementally apply uniaxial strain and perform absorption and PL measurements. We ensure to measure absorption and PL on the same sample location (within the spot size of the light beam, 0.8 μm) for a given strain level.

We perform all the sample fabrication and optical measurements at room temperature and without any other processing. We prefer that in order to minimize uncontrollable strain due to temperature changes, and any other modifications to the samples. Figure S1 demonstrates the effect of transfer on the PL spectra of 1L WSe_2. Redshifts of 6-9 meV are observed. Such redshifts may be attributed to different dielectric screening, increased Stokes shift, and strain ($\lesssim$0.1%) induced during transfer. Spectra for PETG measurements are blueshifted for easier comparison of the measurements on the two substrates. The lineshapes seem very similar before (on PDMS) and after transfer (on PETG) for 3 different regions of the sample.

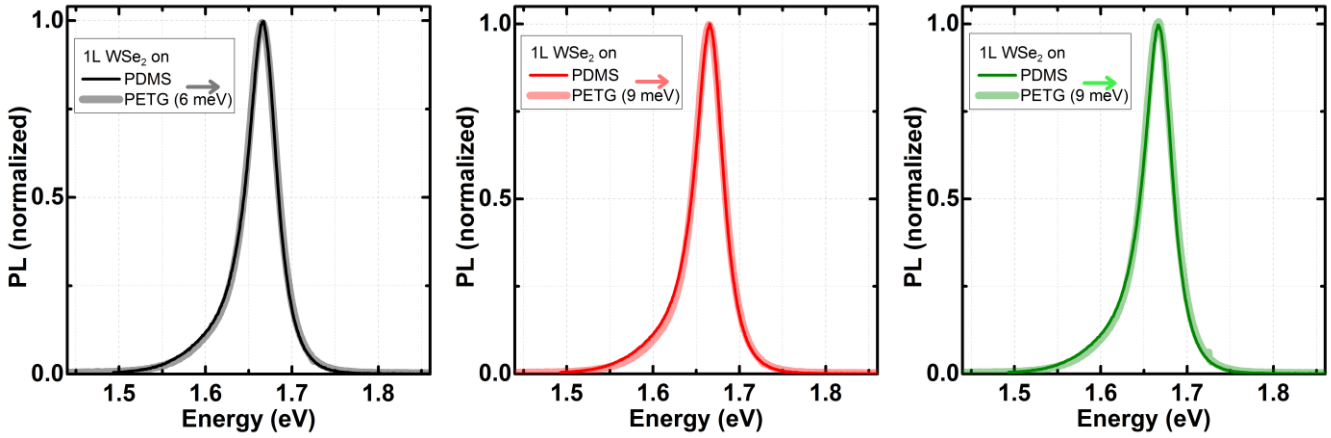


Figure S1: Effect of transferring 1L WSe_2 from PDMS to PETG substrates on the PL lineshape. Spectra measured on PETG are blue shifted by the amounts indicated in each legend to easily compare to the spectra on PDMS.

We calculate the absorption from the linear reflectance contrast, $\Delta R/R = (R_{1L+PETG} - R_{PETG})/R_{PETG}$, where $R_{1L+PETG}$ and R_{PETG} are the reflectance of the monolayer on the PETG substrate and of the bare PETG substrate [52].

For absorption measurements, a tungsten-halogen lamp at a temperature of about 3400 K was focused down to a spot size of about 0.8 µm on the sample. For PL measurements, 1Ls are excited with a 532 nm (2.33 eV) solid-state laser, which was blocked on the optical collection path with a long-pass color filter. A 40× objective with a numerical aperture (NA) of 0.6 was used for all measurements. The collected light was analyzed in a 300 mm focal length spectrometer equipped with a grating of 150 lines/mm blazed at a photon wavelength of 500 nm. We obtained a spectral resolution of 0.8 meV around the peak energy of the A exciton.

Since the PL spectra redshifted with strain, we consider the energy-dependent collection efficiency of the optical elements. Those elements include the following: objective lens, mirrors, beam-splitting cube, long-pass filter, diffraction grating, Si CCD camera. Normalized collection efficiency is plotted in Figure S2. We see that the collection efficiency decreases by about 40% over the spectral range of the strain dependent peak position of the A exciton. We correct the PL spectra accordingly. We stress that such a correction is crucial for accurately determining the strain dependence of PL intensity.

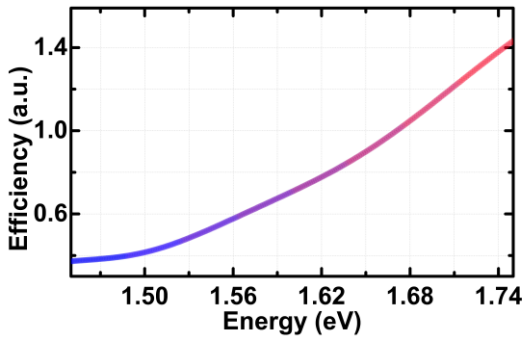


Figure S2: Collection efficiency of the optical path from the sample to the detector. The efficiency is normalized to be 1 at 1.67 eV, the peak energy of the A exciton PL of unstrained 1L WSe_2.

We would also like to comment on the strain-induced PL enhancement for 1L WSe_2 reported by Desai et al. [10]. We note that processing the samples for polymer clamping would result in inhomogeneous broadening which was reflected by the linewidth of larger than 100 meV of unstrained 1L WSe_2. Thus, it is difficult to decouple the effect of strain on the intrinsic properties of the samples from the effect on the interaction between the sample and the environment, which would both affect the PL intensity. For instance, the sample may conform better to the substrate and to the clamping

polymer with increasing strain, eliminating inhomogeneities such as wrinkles. Furthermore, it is difficult to account for the strain-induced changes in the dielectric environment, which also affect the excitonic properties [4]. Thus, we conclude that the lack of a significant PL enhancement in our results is not in contradiction with results reported in the literature.

S2 Applying Strain to PETG and WSe_2, and Its Calculation

We apply strain to the PETG substrate in a symmetric 3-point bending geometry and calculate the strain from the vertical deflection at its center. It is expected that the applied strain on the substrate will not be uniformly transmitted to the 1Ls due to the spatially-varying interfacial shear stress [11,53]. Therefore, we calculate the strain for the individual points measured by assuming a linear relationship between the strain and the optical gap from the maximum optical gap change (100 meV) under the largest strain (2.1%), yielding about 47 meV redshift per % strain. At an applied strain of 1.2% on the substrate, the largest redshift we observe on the sample is 56 meV, which also yields 47 meV redshift per % strain. The linear correlation between the calculated strain and other optical fingerprints such as the splitting between the A exciton, and B exciton and C feature supports our assumption. Figure S3 shows the energy separation between the C feature and A_{1s} exciton which increases linearly from the 0% strain value of 783 meV by 57 meV/% strain.

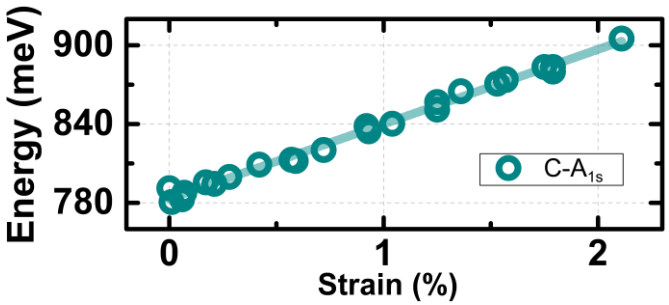


Figure S3: Energy separation between the peak positions of the C feature and A_{1s} exciton (hollow circles) and its linear fit (solid line).

S3 Strain-dependent Absorption Spectra of 1L WSe_2

Figure S4 plots the strain-dependent absorption spectra of 1L WSe_2 ranging from 0.0% to 2.1% strain at various values. Figure S4a clearly shows that the features labeled, namely A_{1s}, A_{2s}, A_{3s}, and B_{1s}, redshift with strain. We plot the same spectra by horizontally shifting them in Figure S4b such that the peak energies of the A_{1s} excitons match. It is clear in Figure S4b that the excited excitonic states of the A exciton, A_{2s}, A_{3s}, are closer to the ground state, A_{1s}, as described in detail in the main text. This closeness with strain is attributed to the smaller reduced mass of the A exciton of the strained 1L resulting in a smaller binding energy. Besides, the blueshift of the B_{1s} exciton relative to the A_{1s} exciton can also be observed in Figure S4b. Such a blueshift is mainly attributed to the increased spin-splitting in the valence band (VB). Therefore, B_{1s} blueshifts by 16(±1) meV/% strain with respect to A_{2s}, making the observation of the latter and other excited states easier.

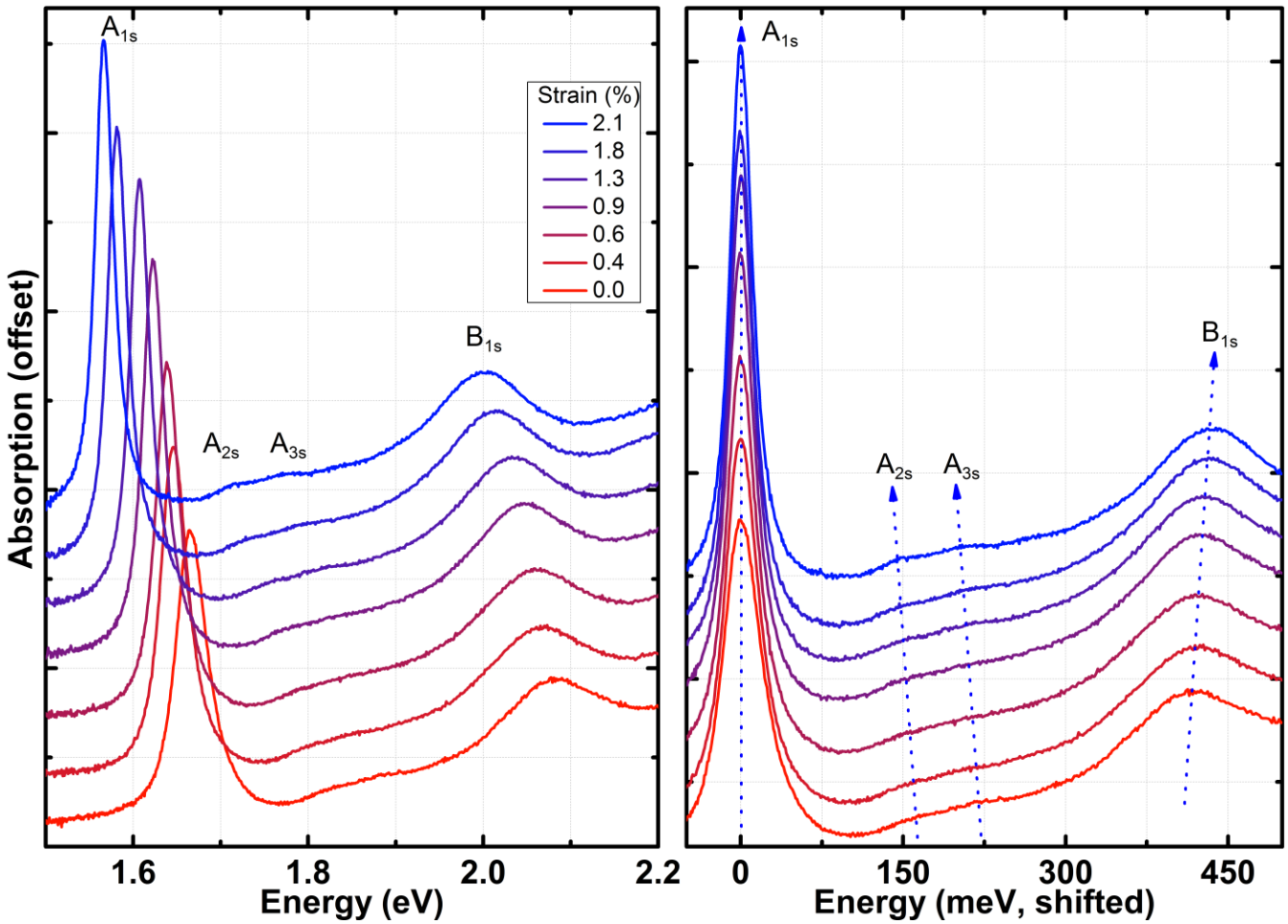


Figure S4: Strain-dependent absorption spectra of 1L WSe_2. Spectra are vertically offset for clarity in (a). Spectra are vertically offset as well as horizontally such that the A_{1s} exciton position relative to the other features observed can be emphasized in (b). The dashed lines in (b) are guides to the eye to track the peak energies of the excitons relative to A_{1s}.

Given that the intensity of absorption due to the A_{1s} exciton is quite insensitive to strain as discussed in the paper, we expect the oscillator strengths of all the excitons to be insensitive to strain. Thus, we fit the absorption spectra to multiple Lorentzian line shapes by keeping the *relative* oscillator strengths of the excitons fixed. We therefore limit the free parameters to the following in the fitting procedure: Oscillator strength of the A_{1s} exciton, positions and the linewidths of all peaks.

S4 Strain Dependence of the KK Quasiparticle Gap for 1L WSe_2

Strain-induced change to the KK quasiparticle gap, E_{KK}, can be expressed as $\Delta E_{KK}^{quasiparticle}(\varepsilon) = \Delta E_{KK}(\varepsilon) + \Delta E_{KK}^{binding}(\varepsilon)$. $\Delta E_{KK}^{quasiparticle}(\varepsilon)$ and $\Delta E_{KK}^{binding}(\varepsilon)$ are changes induced by strain, ε, to KK quasiparticle gap and exciton binding energy, respectively.

For 1L WSe_2, we obtain $\Delta E_{KK}^{quasiparticle}(\varepsilon)$ = -59(±2) meV/% strain for 1L WSe_2, from the values reported in the paper ($\Delta E_{KK}(\varepsilon)$ = -47 meV/% strain, $\Delta E_{KK}^{binding}(\varepsilon)$ = -12(±2) meV/% strain) , which is in good agreement with the calculated value of -60 meV/% strain reported in the supporting information of Ref. [10].

S5 Linewidth as a function of $KQ - KK$ separation for 1L WSe_2 and 1L WS_2

We note that the strain-dependent linewidths of 1L WSe_2 and WS_2 show quite distinct behavior stemming from their different KQ and KK gap separation under 0 % strain, $E_{KQ-KK}(\varepsilon = 0)$. Thus it is valuable to compare the dependence

of linewidths on E_{KQ-KK} under strain as we plot below. E_{KQ-KK} has been calculated from the strain values in Figure 2 and as described in the paper. Thus, we estimate a difference of 60 meV between the two materials for $E_{KQ-KK}(\varepsilon = 0)$ by matching their linewidth data.

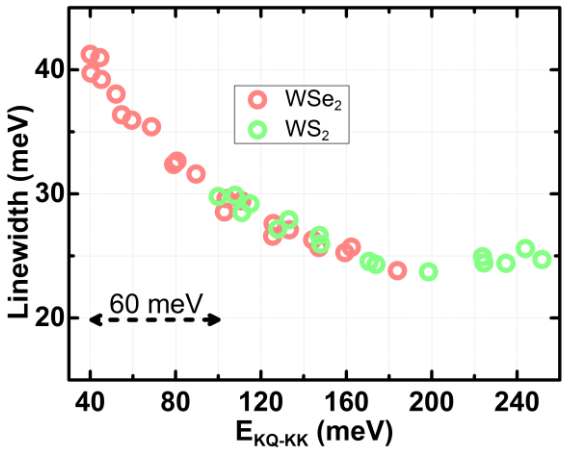


Figure S5: Dependence of the linewidths of the A excitons of 1L WSe_2 and WS_2

S6 $KQ - KK$ Separation for 1L and Few-layer WSe_2

We note that the indirect (direct) gap of few-layer WSe_2 occurs between the K valley of VB and Q (K) valley of CB constituting the KQ (KK) exciton, as in the case of 1L WSe_2 [10,54]. The values of the energy separation between those states, E_{KQ-KK}, were reported to be about -80, -160, and -200 meV for 2L, 3L, and 4L measured via PL spectroscopy, respectively [55,56]. We note that E_{KQ-KK} increases exponentially with layer thickness and no PL is observed from the indirect gap of 1L [54,56]. Thus, our estimate for E_{KQ-KK} in 1L is consistent with the thickness dependence of the KQ and KK gaps reported.

S7 Strain Dependence of the Binding energy of the KQ and B excitons, and B-A splitting

Strain-dependent binding energy of the ground state KQ exciton, $\mathrm{E}_{KQ}^{binding}$, can be estimated by the strain dependence of its reduced mass, m_{KQ}, and comparing to those of the KK exciton of which the strain-dependent binding energy, $\mathrm{E}_{KK}^{binding}$, has been experimentally measured. Assuming that the excitonic binding energy is linearly proportional to the exciton reduced mass and assuming that applying strain does not cause other changes that affect the binding energy, we write the following:

$$\mathrm{E}_{KQ}^{binding}(\varepsilon = 0) = \mathrm{E}_{KK}^{binding}(\varepsilon = 0)\frac{m_{KQ}}{m_{KK}}(\varepsilon = 0)$$

Then, we write the changes to the binding energies of KQ and KK excitons due to the changes in the exciton reduced masses as follows:

$$\Delta E_{KQ}^{binding}(\varepsilon) = \mathrm{E}_{KQ}^{binding}(0)\frac{\Delta m_{KQ}(\varepsilon)}{m_{KQ}(0)}$$

$$\Delta E_{KK}^{binding}(\varepsilon) = \mathrm{E}_{KK}^{binding}(0)\frac{\Delta m_{KK}(\varepsilon)}{m_{KK}(0)}$$

Where m_{KQ} and m_{KK} are the reduced masses of the KQ and KK excitons, respectively. Substituting for $\mathrm{E}_{KQ}^{binding}(0)$ and $\mathrm{E}_{KK}^{binding}(0)$ yields the following:

$$\Delta E_{KQ}^{binding}(\varepsilon) = \Delta E_{KK}^{binding}(\varepsilon)\frac{\Delta m_{KQ}(\varepsilon)}{\Delta m_{KK}(\varepsilon)}$$

Instead of estimating the binding energy of the B exciton from the calculated reduced masses, we use the experimentally observed values: The binding energy of the B exciton of 1L WSe_2 (on SiO_2/Si) has been reported to be about 20% higher than that of the A exciton at a temperature of 5 K [4]. The difference is mainly a result of the different reduced masses and dielectric screening for the two excitons [57]. Assuming that a similar relationship holds in our case and that the reduced mass, thus binding energy, of the B exciton changes at the same relative rate with strain as the A exciton from calculations [36], we can estimate the strain-dependent binding energy of the B exciton to be about 378-14(±2) meV/% strain (=120% × (315-12(±2) meV/% strain)). We then obtain the following:

$$E_B^{binding} - E_A^{binding} = 63\ meV - 2(\pm 1)\ meV\frac{\varepsilon}{\%} \quad (3)$$

where $E_{A\,(B)}^{binding}$ is the binding energy of the A (B) exciton. B exciton is the 2nd lowest energy spin-allowed transition that occurs between the top of the valence and the bottom of the conduction band (CB) at the K point. Thus, E_{B-A} depends on the relative magnitude of the splittings at the K point of VB (E_{VB}^{spin}) and CB (E_{CB}^{spin}) due to spin-orbit coupling and relative binding energies of the A and B excitons, and we express it as follows:

$$E_{B-A} = E_{VB}^{spin} - E_{CB}^{spin} - E_B^{binding} + E_A^{binding} \quad (4)$$

As given in the manuscript, E_{B-A} increases from 409 meV by 10 meV/% strain. Thus, we obtain $E_{VB}^{spin} - E_{CB}^{spin}$= 472 meV + 8(±1) meV/% strain. Theoretical and experimental results have been reported which are in agreement with our estimate of 472 meV for $E_{VB}^{spin} - E_{CB}^{spin}$ [18]. The increase with strain is predicted to be dominated by E_{VB}^{spin}, which is in agreement with the calculated values ranging from 5 to 10 meV/% strain [35,36].

S8 Strain Dependence of Stokes Shift and Estimating the Inhomogeneous Broadening

Given the significant decrease in the linewidth, an important question is what happens to the Stokes shift (SS), the energy difference between the A exciton absorption and emission peaks, since they were proposed to be correlated in quantum-well semiconductors. SS is mainly attributed to localization and thermalization in quantum wells [58-60]. We expect the localization model, recombination of the trapped excitons in localized states, to dominate the SS and result in a band-tail of the PL as observed in our 0% PL spectrum of Figure S6a [59,60]. Such a band-tail in the PL is an indication of inhomogeneity. Moreover, strain is expected to decrease the surface roughness of the 1L on the underlying substrate. Decreased surface roughness will eliminate the local states and reduce the recombination of the band-tail localized exciton at the lower energy side of the PL [59]. This effect is reflected by the more-symmetric PL spectrum of strained 1L compared to unstrained 1L as shown in Figure S6a. SS decreases from about 7 meV to 3 meV with increasing strain (Figure S6b) as accompanied by the suppression of the localized exciton PL emission. To account for the decrease in the inhomogeneous broadening of the A exciton absorption peak and isolate the decrease in the homogeneous broadening, we estimate the linewidth due to inhomogeneous broadening to be equal to SS. We calculate the homogeneous broadening from the total linewidth by assuming a Voigt linewidth (Figure S6c) [61]. We note that the effect of the decrease in the inhomogeneous linewidth on the total linewidth is rather small. We observed similar results from WS_2 and accounted for its inhomogeneous broadening.

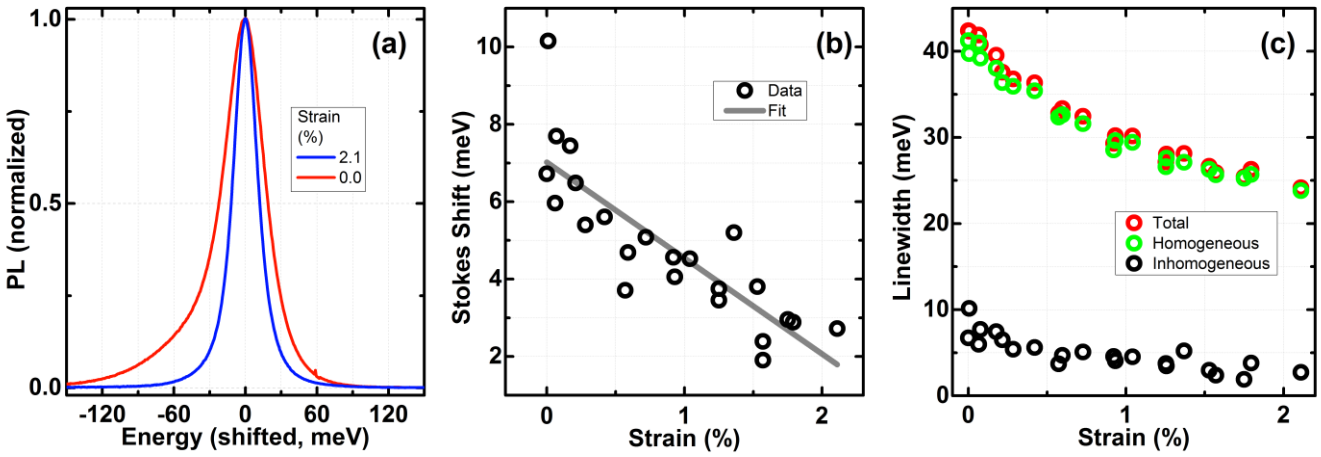


Figure S6: (a) PL spectra at 2.1% and 0% strain (horizontally shifted and normalized for clarity). (b) Stokes Shift in 1L WSe_2 with increasing strain. (c) Total, homogeneous and inhomogeneous linewidths of the A_{1s} exciton absorption peak of 1L WSe_2 as a function of strain.

S9 Effect of hBN Encapsulation on the Exciton Linewidths

We also hope to shed light on the underlying mechanism of the linewidth decrease in hBN encapsulated 1Ls, which has been attributed to the elimination of inhomogeneities [44,62].

It has been recently discovered that hBN encapsulation reduces the linewidths of 1L TMDCs and this effect has been attributed to the elimination of inhomogeneities [44,62]. The inhomogeneities that can be eliminated by hBN are not expected to be different for different TMDCs, but the observation that hBN encapsulation results in different quantitative reductions on the linewidths of, for example, MoS_2 and WS_2 indicates that additional mechanisms may be playing a role. Therefore, it is crucial to study the effect of hBN on the band structure and other properties affecting the exciton-phonon scattering in TMDCs to distinguish the proposed elimination of inhomogeneities from any other modifications [63-65].

S10 Orientation Dependence of Applied Strain

We note that within the regime of (relatively low) strain we have examined in this study, we expect no significant dependence of the material properties on the direction of the axis of the strain relative to the crystallographic axes of the monolayer [38,39,66]

S11 Built-in or Temperature-Driven Strain, Dielectric Screening

Our results show that the excitonic features in TMDCs are sensitive to the variations in the band structure. Therefore, the compressive strain-like effect of the low temperature as well as any built-in strain due to the sample fabrication and the dielectric environment should be taken into account to correctly interpret the experimental results obtained from TMDCs. For instance, E_{KQ-KK} will decrease with decreasing temperature and "a more indirect gap" is expected from 1L WSe_2 at low temperature [29,31]. In fact, it was reported that the indirect and direct gaps shift at different rates with temperature in few-layer TMDCs [55]. Thus, intervalley scattering will be strongly influenced by the temperature-dependent energy separation of those gaps. We note that a recent STM study reported an indirect gap for WSe_2 [29]. However, the band structure of the samples that were investigated is expected to be different from those we used in our study due to the different experimental conditions: Dielectric environment and temperature. Furthermore, STM is capable of probing all electronic spin states as opposed to the optically-bright excitonic states that we examine. Therefore, the direct gap we report for WSe_2 is not inconsistent with that study.

References

[1] A. Chernikov, T. C. Berkelbach, H. M. Hill, A. Rigosi, Y. Li, O. B. Aslan, D. R. Reichman, M. S. Hybertsen, and T. F. Heinz, Phys. Rev. Lett. **113**, 076802 (2014).

[2] K. He, N. Kumar, L. Zhao, Z. Wang, K. F. Mak, H. Zhao, and J. Shan, Phys. Rev. Lett. **113**, 026803 (2014).

[3] A. Chernikov, A. M. van der Zande, H. M. Hill, A. F. Rigosi, A. Velauthapillai, J. Hone, and T. F. Heinz, Phys. Rev. Lett. **115**, 126802 (2015).

[4] A. Raja, A. Chaves, J. Yu, G. Arefe, H. M. Hill, A. F. Rigosi, T. C. Berkelbach, P. Nagler, C. Schuller, T. Korn, C. Nuckolls, J. Hone, L. E. Brus, T. F. Heinz, D. R. Reichman, and A. Chernikov, Nat. Commun. **8**, 15251 (2017).

[5] A. V. Stier, N. P. Wilson, G. Clark, X. D. Xu, and S. A. Crooker, Nano Lett. **16**, 7054 (2016).

[6] G. Gupta, S. Kallatt, and K. Majumdar, Phys. Rev. B **96**, 081403 (2017).

[7] A. V. Stier, N. P. Wilson, K. A. Velizhanin, J. Kono, X. Xu, and S. A. Crooker, Phys. Rev. Lett. **120**, 057405 (2018).

[8] D. Lloyd, X. H. Liu, J. W. Christopher, L. Cantley, A. Wadehra, B. L. Kim, B. B. Goldberg, A. K. Swan, and J. S. Bunch, Nano Lett. **16**, 5836 (2016).

[9] H. J. Conley, B. Wang, J. I. Ziegler, R. F. Haglund, S. T. Pantelides, and K. I. Bolotin, Nano Lett. **13**, 3626 (2013).

[10] S. B. Desai, G. Seol, J. S. Kang, H. Fang, C. Battaglia, R. Kapadia, J. W. Ager, J. Guo, and A. Javey, Nano Lett. **14**, 4592 (2014).

[11] R. Schmidt, I. Niehues, R. Schneider, M. Druppel, T. Deilmann, M. Rohlfing, S. M. de Vasconcellos, A. Castellanos-Gomez, and R. Bratschitsch, 2D Mater. **3**, 021011 (2016).

[12] J. T. Ji, A. M. Zhang, T. L. Xia, P. Gao, Y. H. Jie, Q. Zhang, and Q. M. Zhang, Chin. Phys. B **25**, 077802 (2016).

[13] K. He, C. Poole, K. F. Mak, and J. Shan, Nano Lett. **13**, 2931 (2013).

[14] J. O. Island, A. Kuc, E. H. Diependaal, R. Bratschitsch, H. S. J. van der Zant, T. Heine, and A. Castellanos-Gomez, Nanoscale **8**, 2589 (2016).

[15] G. H. Ahn, M. Amani, H. Rasool, D. H. Lien, J. P. Mastandrea, J. W. Ager, M. Dubey, D. C. Chrzan, A. M. Minor, and A. Javey, Nat. Commun. **8**, 608 (2017).

[16] I. Niehues, R. Schmidt, M. Druppel, P. Marauhn, D. Christiansen, M. Selig, G. Berghauser, D. Wigger, R. Schneider, L. Braasch, R. Koch, A. Castellanos-Gomez, T. Kuhn, A. Knorr, E. Malic, M. Rohlfing, S. Michaelis de Vasconcellos, and R. Bratschitsch, Nano Lett. **18**, 1751 (2018).

[17] O. B. Aslan, I. M. Datye, M. J. Mleczko, K. Sze Cheung, S. Krylyuk, A. Bruma, I. Kalish, A. V. Davydov, E. Pop, and T. F. Heinz, Nano Lett. **18**, 2485 (2018).

[18] A. Kormanyos, G. Burkard, M. Gmitra, J. Fabian, V. Zolyomi, N. D. Drummond, and V. Fal'ko, 2D Mater. **2**, 022001 (2015).

[19] Z. H. Jin, X. D. Li, J. T. Mullen, and K. W. Kim, Phys. Rev. B **90**, 045422 (2014).

[20] M. Hosseini, M. Elahi, M. Pourfath, and D. Esseni, IEEE Trans. Electron Devices **62**, 3192 (2015).

[21] X. Li, J. T. Mullen, Z. Jin, K. M. Borysenko, M. Buongiorno Nardelli, and K. W. Kim, Phys. Rev. B **87**, 115418 (2013).

[22] M. Selig, G. Berghauser, A. Raja, P. Nagler, C. Schuller, T. F. Heinz, T. Korn, A. Chernikov, E. Malic, and A. Knorr, Nat. Commun. **7**, 13279 (2016).

[23] K. Kaasbjerg, K. S. Thygesen, and K. W. Jacobsen, Phys. Rev. B **85**, 115317 (2012).

[24] M. Hosseini, M. Elahi, M. Pourfath, and D. Esseni, Appl. Phys. Lett. **107**, 253503 (2015).

[25] C. E. P. Villegas and A. R. Rocha, J. Phys. Chem. C **119**, 11886 (2015).

[26] S. H. Rhim, Y. S. Kim, and A. J. Freeman, Appl. Phys. Lett. **107**, 241908 (2015).

[27] M. A. U. Absor, H. Kotaka, F. Ishii, and M. Saito, Phys. Rev. B **94**, 115131 (2016).

[28]

[29] C. D. Zhang, Y. X. Chen, A. Johnson, M. Y. Li, L. J. Li, P. C. Mende, R. M. Feenstra, and C. K. Shih, Nano Lett. **15**, 6494 (2015).

[30] W. T. Hsu, L. S. Lu, D. Wang, J. K. Huang, M. Y. Li, T. R. Chang, Y. C. Chou, Z. Y. Juang, H. T. Jeng, L. J. Li, and W. H. Chang, Nat. Commun. **8**, 929 (2017).

[31] J. Lindlau, C. Robert, V. Funk, J. Förste, M. Förg, L. Colombier, A. Neumann, E. Courtade, S. Shree, T. Taniguchi, K. Watanabe, M. M. Glazov, X. Marie, B. Urbaszek, and A. Högele, arXiv:1710.00988.

[32] M. Feierabend, A. Morlet, G. Berghauser, and E. Malic, Phys. Rev. B **96**, 045425 (2017).

[33] H. L. Shi, H. Pan, Y. W. Zhang, and B. I. Yakobson, Phys. Rev. B **87**, 155304 (2013).

[34] T. Berkelbach (private communication).

[35] D. Le, A. Barinov, E. Preciado, M. Isarraraz, I. Tanabe, T. Komesu, C. Troha, L. Bartels, T. S. Rahman, and P. A. Dowben, J. Phys. Condens. Matter **27**, 182201 (2015).
[36] B. Amin, T. P. Kaloni, and U. Schwingenschlogl, RSC Adv. **4**, 34561 (2014).
[37] G. Moody, C. K. Dass, K. Hao, C. H. Chen, L. J. Li, A. Singh, K. Tran, G. Clark, X. D. Xu, G. Berghauser, E. Malic, A. Knorr, and X. Q. Li, Nat. Commun. **6**, 8315 (2015).
[38] A. M. Dadgar, D. Scullion, K. Kang, D. Esposito, E.-H. Yang, I. P. Herman, M. A. Pimenta, E.-J. G. Santos, and A. N. Pasupathy, Chem. Mater. **30**, 5148 (2018).
[39] C. H. Chang, X. F. Fan, S. H. Lin, and J. L. Kuo, Phys. Rev. B **88**, 195420 (2013).
[40] O. B. Aslan, Y. Yu, L. Cao, and M. Brongersma, (unpublished).
[41] A. R. Goni, A. Cantarero, K. Syassen, and M. Cardona, Phys. Rev. B **41**, 10111 (1990).
[42] G. H. Li, A. R. Goni, K. Syassen, and M. Cardona, Phys. Rev. B **49**, 8017 (1994).
[43] I. Bernal-Villamil, G. Berghauser, M. Selig, I. Niehues, R. Schmidt, R. Schneider, P. Tonndorf, P. Erhart, S. M. de Vasconcellos, R. Bratschitsch, A. Knorr, and E. Malic, 2D Mater. **5**, 025011 (2018).
[44] F. Cadiz, E. Courtade, C. Robert, G. Wang, Y. Shen, H. Cai, T. Taniguchi, K. Watanabe, H. Carrere, D. Lagarde, M. Manca, T. Amand, P. Renucci, S. Tongay, X. Marie, and B. Urbaszek, Phys. Rev. X **7**, 021026 (2017).
[45] J. Lee, J. S. Huang, B. G. Sumpter, and M. Yoon, 2D Mater. **4**, 021016 (2017).
[46] W. Wei, Y. Dai, C. W. Niu, and B. B. Huang, Sci. Rep. **5**, 17578 (2015).
[47] D. M. Guzman and A. Strachan, J. Appl. Phys. **115**, 243701 (2014).
[48] H. Kumar, D. Q. Er, L. Dong, J. W. Li, and V. B. Shenoy, Sci. Rep. **5**, 10872 (2015).
[49] S. Pak, J. Lee, Y. W. Lee, A. R. Jang, S. Ahn, K. Y. Ma, Y. Cho, J. Hong, S. Lee, H. Y. Jeong, H. Im, H. S. Shin, S. M. Morris, S. Cha, J. I. Sohn, and J. M. Kim, Nano Lett. **17**, 5634 (2017).
[50] M. V. Fischetti and S. E. Laux, J. Appl. Phys. **80**, 2234 (1996).
[51] S. Bertolazzi, J. Brivio, and A. Kis, ACS Nano **5**, 9703 (2011).
[52] O. B. Aslan, Ph.D., Columbia University, 2017.
[53] T. Jiang, R. Huang, and Y. Zhu, Adv. Funct. Mater. **24**, 396 (2014).
[54] H. L. Zeng, G. B. Liu, J. F. Dai, Y. J. Yan, B. R. Zhu, R. C. He, L. Xie, S. J. Xu, X. H. Chen, W. Yao, and X. D. Cui, Sci. Rep. **3**, 1608 (2013).
[55] W. J. Zhao, R. M. Ribeiro, M. L. Toh, A. Carvalho, C. Kloc, A. H. C. Neto, and G. Eda, Nano Lett. **13**, 5627 (2013).
[56] W. Zhao, Z. Ghorannevis, L. Chu, M. Toh, C. Kloc, P.-H. Tan, and G. Eda, ACS Nano **7**, 791 (2013).
[57] T. C. Berkelbach, M. S. Hybertsen, and D. R. Reichman, Phys. Rev. B **88**, 045318 (2013).
[58] A. Polimeni, A. Patane, M. Grassi Alessi, M. Capizzi, F. Martelli, A. Bosacchi, and S. Franchi, Phys. Rev. B **54**, 16389 (1996).
[59] A. Ait-Ouali, R. Y. F. Yip, J. L. Brebner, and R. A. Masut, J. Appl. Phys. **83**, 3153 (1998).
[60] A. Ait-Ouali, J. L. Brebner, R. Y. F. Yip, and R. A. Masut, J. Appl. Phys. **86**, 6803 (1999).
[61] F. Yang, M. Wilkinson, E. J. Austin, and K. P. O'Donnell, Phys. Rev. Lett. **70**, 323 (1993).
[62] O. A. Ajayi, J. V. Ardelean, G. D. Shepard, J. Wang, A. Antony, T. Taniguchi, K. Watanabe, T. F. Heinz, S. Strauf, X. Y. Zhu, and J. C. Hone, 2D Mater. **4**, 031011 (2017).
[63] Z. Y. Huang, C. Y. He, X. Qi, H. Yang, W. L. Liu, X. L. Wei, X. Y. Peng, and J. X. Zhong, J. Phys. D Appl. Phys. **47**, 075301 (2014).
[64] M. K. L. Man, S. Deckoff-Jones, A. Winchester, G. S. Shi, G. Gupta, A. D. Mohite, S. Kar, E. Kioupakis, S. Talapatra, and K. M. Dani, Sci. Rep. **6**, 20890 (2016).
[65] C. Yelgel, O. C. Yelgel, and O. Gulseren, J. Appl. Phys. **122**, 065303 (2017).
[66] C. R. Zhu, G. Wang, B. L. Liu, X. Marie, X. F. Qiao, X. Zhang, X. X. Wu, H. Fan, P. H. Tan, T. Amand, and B. Urbaszek, Phys. Rev. B **88**, 121301 (2013).